



# Effect of surface morphology on the sputtering yields. I. Ion sputtering from self-affine surfaces

Maxim A. Makeev<sup>\*</sup>, Albert-László Barabási

*Department of Physics, University of Notre Dame, Notre Dame, IN 46566, USA*

Received 20 August 2003; received in revised form 16 February 2004

## Abstract

As extensive experimental studies have shown, under certain conditions, ion bombardment of solid targets induces a random (self-affine) morphology on the ion-eroded surfaces. The rough morphology development is known to cause substantial variations in the sputtering yields. In this article, we present a theoretical model describing the sputter yields from random, self-affine surfaces subject to energetic ion bombardment. We employ the Sigmund's theory of ion sputtering, modified for the case of self-affine surfaces, to compute the sputter yields. We find that the changes in the sputtering yield, associated with the non-planar surface morphology, are strongly dependent on the parameters characterizing the surface roughness (such as the saturation width and the correlation length) and the incident ion beam (such as the incident ion energy and the deposited energy widths). It is shown that, for certain ranges of the parameters variations, surface roughness leads to substantial enhancements in the yield, with magnitude of the effect being more than 100%, as compared to the flat surface value. Furthermore, we find that, depending on the interplay between these parameters, the surface roughness can both enhance and suppress the sputter yields.

© 2004 Elsevier B.V. All rights reserved.

PACS: 68.35.C; 34.50.D; 81.65.C; 79.20.R

## 1. Introduction

Ion-bombardment of solid surfaces with energetic ions is known to cause sputtering of atoms from the target surfaces and often leads to the development of a number of non-trivial surface

morphologies. The general interest in the phenomenon of sputter erosion stems from its extensive use in a variety of applications related to the surface analysis. These applications include, but not limited to, secondary ion mass spectroscopy (SIMS), Auger electron microscopy (AES) and the X-ray photoelectron spectroscopy (XPS). A successful application of these techniques requires a detailed knowledge of the processes taking place at the surfaces of ion-eroded materials. Although significant progress has been made in understanding the interaction of energetic particles with solid targets, there still exists a number of unresolved issues including those related to the

<sup>\*</sup> Corresponding author. Present address: Collaboratory for Advanced Computing and Simulations, Department of Materials Science and Engineering, University of Southern California, VHE 608, 3651 Watt Way, Los Angeles, CA 90089-0242, USA. Tel.: +1-213-821-2661; fax: +1-213-821-2664.

E-mail addresses: [makeev@usc.edu](mailto:makeev@usc.edu) (M.A. Makeev), [alb@nd.edu](mailto:alb@nd.edu) (A.-L. Barabási).

secondary ion yields changes in the SIMS and, associated with these changes, depth profile degradation, which is known to occur when the surface roughness is developed. In the light of technological importance of SIMS, many experimental as well as theoretical studies have been focused on the problem of surface profile degradation and the secondary ion yield changes, taking place during erosion of surfaces with a non-planar morphology. For a better control of this technique, it is essential to either find a way to predict accurately the sputtering yields from rough surfaces or to suppress the roughness development. Up to now, an accurate correction procedure accounting for the ion yield changes in SIMS was not developed due to a complex character of the problem. On the other hand, the experimental observations suggest that the surface morphology development leads to considerable modifications in the sputter yields. A number of studies of the effect of the surface roughness on the sputter yield behavior were undertaken, with particular emphasis on the surfaces with ripple morphology [4–16]. It is well understood by now that the observed sputter yield variations are caused by the development of the ripple morphology on the ion-eroded surfaces [6,11,13,16], in which case the surface roughness development may result in more than 100% large sputtering yield enhancements. Moreover, a number of studies have shown that the ripple formation can be suppressed by sample rotation [4,9]. In this case no sputter yield changes were observed. Based upon the theory of ripple formation, due to Bradley and Harper [17], a theoretical explanation of the effect of sample rotation on the ripple structure was given in [18,19].

Recently, a number of studies of morphology of the ion-bombarded surfaces were undertaken, which allowed to conclude that, under certain experimental conditions, target surfaces can undergo kinetic roughening, with resultant surfaces being random and possessing the self-affine properties. Experimental [20–28] and theoretical [29–44] studies, focusing on the characterization of the rough surfaces, have provided the basis for development of the tools adequately describing the self-affine surfaces. As a result, by now there exists

extensive experimental evidence that the ion-sputtered surfaces may develop the self-affine profiles, which can be adequately described by the existing theoretical concepts involving the fractal geometries. Thus, it is understood that the rough morphology of the self-affine interfaces can be described in terms of the surface width and the correlation length [30]. The applicability of the scaling theory to the description of the rough surfaces was verified by extensive experimental studies performed with different materials, including graphite [20,21], iron [22] and Si [23]. These studies were complemented by atomistic simulations of the ion-bombardment process, which allowed for the microscopic level of understanding of the mechanisms governing the surface roughness development and evolution. The surface ripple characteristics and the kinetic roughening exponents were computed in [45–48] and compared with experimental data and theoretical results, thus validating the concepts uncovered in experimental studies and continuum-description-based theoretical models.

Although numerous experimental investigations show that the surface roughness leads to considerable modifications of the sputtering yields, there is no analytical theory, which would account for this effect. Indeed, the classical theoretical literature, focusing on the ion sputtering, is based upon the *flat surface approximation*, thus completely ignoring the surface roughness [1–3]. It should be noted, however, that a number of Monte Carlo simulation based studies were performed to study the effect and provided an invaluable information on the process of sputtering of the rough surfaces [49–51]. On the other hand, such studies are not portable and does not allow to investigate sufficiently large number of surface profile configurations, which affects the limit of applicability of such computer-based models. An analytical model is required, which would allow for calculating the sputter yields for any target material, bombarded under various experimental conditions. As we show below, development of such model is feasible due to the universal character of the roughness exponents.

In this article, we provide a detail discussion of our model of the ion sputtering from random,

self-affine surfaces, which allows us to investigate the influence of the surface roughness on the sputtering yields. A short account of the model was previously reported on in [52]. In the following, we discuss various details of our approach and further the discussion of the effect of target surface roughness on the sputter yields. In our model, we envisage the rough surfaces of target materials as fractal-like structures with random modulations of height, being fully characterized by the surface width and the correlation length. These two are well defined quantities, *measurable in experiment* [30]. The case of rippled surfaces is considered in a separate publication [53]. In the basis of our model is the expression for the deposited energy distribution, released by an incoming ion inside the bulk of a target material, adopted from the Sigmund's theory of ion sputtering. This theory is known to work reasonably well, from both qualitative and quantitative points of view, for amorphous targets in the experimentally relevant range of energies from 1 to 100 keV [54]. Our model does not include the case of low-energy sputtering and the limitations thereof are defined by those coming from the Sigmund's theory [54,55]. Using the Sigmund's theory, we obtain an analytical expression for the sputtering yield as a function of the parameters characterizing the incoming ion beam and the target material surface. A combination of numerical and analytical methods is used to investigate the behavior of the yield as a function of the parameters characterizing the roughness of the ion-eroded surfaces (such as the saturation width and correlation length) and the ion bombardment process (such as the incident ion penetration depth and the widths of the deposited energy distributions). We find that the surface roughness can substantially modify the sputtering yields, with magnitude of the effect being dependent on a complex interplay between the parameters characterizing the surface roughness and the incident ion beam. Our results allow us to make rather specific predictions regarding the effect of the surface roughness on the yield, and we discuss the conditions under which they can be tested experimentally. In particular, we show that the flat-surface approximation (used in all previous analytical works) cannot be used to describe the

rough surfaces even in the first approximation since the roughness-induced yield variations can be larger than 100%. Note that qualitatively similar results were obtained in the case of rippled surfaces. In the latter case, we directly confronted our theory with experimental results on the sputter yield changes, taking place during the ion bombardment of the rippled surfaces, and observed that all the major features of the yield behavior are in qualitative agreement with experiments. In some cases, there is also a quantitative agreement between our results and experiments data [58]. This fact as well as some indirect experimental observations allow us to conclude that the presented here model describes well the process of ion sputtering from random surfaces and can be of some value to experimentalists working with the ion-erosion-based techniques.

The rest of the article is organized as follows. Section 2 is devoted to discussion of the theoretical models describing the self-affine morphologies of the rough surfaces. This includes the aspects of kinetic roughening theory and methods of characterization of the self-affine surfaces. Next, in Section 3, we shortly overview the results of experimental studies devoted to the ion-induced kinetic roughening and characterization of the self-affine morphologies. A brief overview of the Sigmund's theory of ion sputtering, including the discussion of the limits of applicability of this theory, is given in Section 4. In Section 5, we derive the equation describing the sputter yield in the case of random (self-affine) surfaces. Further, in Section 6, we concentrate on discussion of the obtained results, which are compared with available experimental data and previously reported results of the atomistic modeling studies. Finally, the main results of our study are briefly summarized in Section 7.

## 2. Scaling theory

The recent advances in the field of fractals, associated with the advent of modern concepts of fractal geometry, universality classes, and scaling, provided the necessary theoretical basis for studying both the steady-state surface morphologies and

their time evolution. The major breakthrough in understanding of the temporal evolution of non-equilibrium interfaces is associated with derivation of the Kardar–Parisi–Zhang (KPZ) equation, which was shown to adequately describe various aspects of the steady-state surface morphologies and their time evolution [32]. The KPZ equation describes the temporal evolution of a surface profile  $h(x, y, t)$ , under growth (or erosion) conditions, and have the following form:

$$\frac{\partial h}{\partial t} = v\nabla^2 h(x, y, t) + \frac{\lambda}{2} (\nabla h(x, y, t))^2 + \eta(x, y, t). \quad (1)$$

The first term on the *rhs* describes the relaxation of an interface due to the surface tension,  $v$ , while the second is a generic non-linear term incorporating the interface growth or erosion. This term arise as the lowest-order correction in the evolving interface velocity expansion in the local surface profile gradients (i.e.  $\partial h/\partial t = v\sqrt{[1 + (\nabla h)^2]}$ ), and is expected to appear in the systems undergoing lateral growth [32]. Further details on derivation of the KPZ equation, including concise discussion of the origin of the non-linear term, are available in [32]. The stochastic noise  $\eta(x, y, t)$  reflects the random fluctuations in the growth process and is given by an uncorrelated random number that has zero configurational average.

The steady-state morphology and dynamics of a rough surface can be characterized by the *interface width*, defined by the *rms* fluctuation in the height of an interface profile,  $h(x, y, t)$ ,

$$w(L, t) \equiv \sqrt{\frac{1}{L^2} \sum_{x,y=1,L} [h(x, y, t) - \bar{h}(t)]^2}, \quad (2)$$

where  $L$  is the linear dimension of the sample. The *mean height* of the surface profile,  $\bar{h}(t)$ , is defined as

$$\bar{h}(t) \equiv \frac{1}{L^2} \sum_{x,y=1,L} h(x, y, t). \quad (3)$$

One of the most important general properties of the self-affine surfaces is that they demonstrate the roughness dependence on the length scale of observation. Consequently, instead of measuring the roughness of a surface over the whole sample,

with linear sizes  $L \times L$ , we can choose a window of size  $\ell \times \ell$  ( $\ell \leq L$ ) and measure  $w(\ell)$ . This can be quantified by plotting  $w(\ell)$  as a function of  $\ell$ . There are two characteristic regimes in the surface width's behavior, one can distinguish, depending on the characteristic length,  $\xi$ .

(i) For length scales smaller than  $\xi$ , i.e. for  $\ell \leq \xi$ , the local surface width increases following

$$w(\ell) = A\ell^\alpha, \quad (4)$$

where  $\alpha$  is the *roughness exponent* and  $A$  is a material dependent proportionality constant. If we are interested in surface phenomena, that take place at the length scales shorter than  $\xi$ , then we cannot neglect the roughness of the surface. In this regime the measure of the roughness is not simply a number, but it depends on the length scale available to the method probing the surface.

(ii) When  $\ell \geq \xi$ ,  $w(\ell)$  is independent of  $\ell$ . For most processes, that take place at length scales larger than  $\xi$ , the surface is considered to be *smooth*, i.e. we can neglect its roughness. In this regime, the surface roughness is characterized with a single number, namely the saturation value of the surface width,  $w_{\text{sat}}$ . In general, reporting a *number* for characterizing the surface roughness, as is frequently done, is a misleading and unsatisfactory procedure. The concept of roughness, for many application, has to be replaced with the length scale dependent roughness, which require the determination of the full  $w(\ell)$  curve. In the short time limit, dynamics of the roughening process is described by the total width, increasing as  $w(L, t) \sim t^\beta$ , where  $\beta$  is the *growth exponent*.

(iii) The scaling properties emerging in (i) and (ii) can be collapsed into a single scaling relation of the form [30]

$$w(r, \xi) \equiv w_{\text{sat}} \left( \frac{r}{\xi} \right)^\alpha f \left( \frac{r}{\xi} \right), \quad (5)$$

where  $w_{\text{sat}}$  is the saturation value of the surface roughness, and  $\xi$  is the correlation length of the height–height correlation function. The scaling function in Eq. (5) possess the following properties:  $f(u \rightarrow \infty) = u^{-\alpha}$  and  $f(u \rightarrow 0) = 1$ . The correlation length scales with time following  $\xi \sim t^z$ , where  $z = \alpha/\beta$  is the *dynamic* exponent.

Studying the scaling relations, such as Eq. (5), allows us to define *universality* classes. The universality class concept is an important product of the modern statistical mechanics, which codifies the fact that there are but a few essential factors that determine the exponents characterizing the scaling behavior. Thus, different systems, which at the first sight may appear to have no connection between them whatsoever, behave in a remarkably similar fashion. The values of the exponents  $\alpha$  and  $\beta$  are independent of many “details” of the system. They are universal, i.e. they do not depend on the details of the crystal lattice or on the implementation of the model, as long as the mechanism generating the roughening does not change. On the contrary, other quantities, such as  $A$ ,  $\xi$  or  $w_{\text{sat}}$ , are non-universal, i.e. they depend on almost every detail of the system. Thus, the characterization of the self-affine surfaces require a knowledge of the scaling exponents.

The scaling exponents can be calculated from the KPZ equation (see Eq. (1)), for surfaces of different dimensions. Thus, in one-dimensional case, the scaling exponents of the KPZ equation can be obtained *exactly*, as  $\alpha = 1/2$ ,  $\beta = 1/3$  and  $z = 3/2$ . However, for higher dimensions they are known only from numerical simulations. For the physically most relevant two-dimensional interface, we obtain  $\alpha \simeq 0.38$  and  $\beta \simeq 0.18$  [33,38].

If, in Eq. (1),  $\lambda = 0$  the remaining equation describes the equilibrium fluctuations of an interface. This equation, was introduced and studied in the context of interface roughening by Edwards and Wilkinson (EW) [39]. It can be solved exactly for an arbitrary dimension due to its linear character, giving the scaling exponents  $\alpha = (2 - d)/2$  and  $\beta = (2 - d)/4$ . For two-dimensional surfaces, we have  $\alpha = \beta = 0$ , leading to the logarithmic roughening of the interface.

The anisotropic version of Eq. (1) was studied by Villain [40], and, subsequently, its properties have been further investigated by Wolf and Villain [42]. The AKPZ equation has different scaling properties depending on signs of the coefficients  $\lambda_x$  and  $\lambda_y$ . Thus, when  $\lambda_x \lambda_y \leq 0$ , a surface is described by the AKPZ equation, and possess the same scaling properties as the EW equation. However, when  $\lambda_x \lambda_y \geq 0$ , the scaling properties are equiva-

lent to the ones provided by the isotropic KPZ equation. The relevance of the AKPZ equation to the sputter erosion was first pointed out by Bruinsma [44].

The effect of surface diffusion on the relaxation of growing interfaces can be incorporated within the framework of Kuramoto–Sivashinsky (KS) equation-based description of growing interfaces [34–36]. In one dimension and for long time and length scales, the isotropic version of the KS equation was shown to exhibit scaling behavior similar to that observed for the KPZ equation, i.e. it demonstrates the self-affine roughening with  $z = 3/2$  and  $\beta = 1/3$ . On the other hand, in the short time scales limit, it shows a pattern formation, with surface morphology reminiscent of ripples. The behavior of the KS equation in two dimensions is not clear. The scaling analysis of a noisy version of the KS equation for one- and two-dimensional evolving interfaces have shown that, in the limit of long time and length scales, its behavior is similar to that described by KPZ equation [37]. It must be noted, however, that the two-dimensional results were obtained only via numerical simulations [37]. These results are also not conclusive, as in the case of the deterministic KS equation.

### 3. Experimental studies of ion-induced roughening

Recently, a number of experimental studies of the roughening process, taking place at the surfaces of ion-bombarded materials, were performed. It was shown that, under certain experimental conditions, the ion-eroded surfaces undergo a kinetic roughening and their properties can be described by the kinetic roughening theory. In the following, we give an overview of some representative works, discussing the surface morphology modifications by the ion-erosion process.

The surface morphology evolution of pyrolytic graphite, bombarded with 5 keV Ar<sup>+</sup> ions, reaching the surface at the angle of incidence,  $\theta = 45^\circ$ , have been reported by Eklund et al. [20]. Using the scanning tunneling microscopy (STM), it was found that the ion-eroded surfaces become rough, with the scaling exponents being  $\alpha \simeq 0.2$ – $0.4$  and

$z \simeq 1.6\text{--}1.8$ . These values are consistent with the theoretical predictions, based upon the KPZ equation [32,33]. It was pointed out, however, that the character of the morphological changes is strongly dependent on the conditions of ion bombardment, such as the ion flux, the ion fluence and the sample temperature. Subsequently, Krim et al. [22] reported their results on 5-keV Ar<sup>+</sup>-ion sputtering of iron, with the angle of incidence of the primary ions being 25°. The surface morphology evolution was monitored via STM. It was found that the eroded surfaces become rough in the course of ion bombardment, with the roughness exponent being  $\alpha \simeq 0.53 \pm 0.02$  [22]. The mechanism leading to such roughness exponent is not understood yet in terms of the continuum theories (two-dimensional growth equations predict the exponents 0.38, 2/3 and 1, all far from the observed value). Moreover, Yang et al. [23] investigated the time evolution of Si(1 1 1) surfaces bombarded with 0.5 keV Ar<sup>+</sup> primary ions, in the temperature range from 300 to 650 °C, using the high-resolution low-energy electron diffraction technique. It was found that, for temperatures below 450 °C, the height–height correlation function shows an anomalous behavior on the short-range scales, with the observed scaling being  $\sim \ln(t)r^{2\alpha}$ . The authors suggested that this anomaly can be explained in terms of a dynamical phase transition. The effect of the surface relaxation (i.e. thermally activated surface diffusion) on the ion-bombardment-induced roughening of GaAs(1 1 0) surfaces, eroded with 2-keV high-purity Ar<sup>+</sup>- and Xe<sup>+</sup>-ions, was reported by Wang et al. [24]. The authors found that both the height–height correlation function and the small-scale roughness increase significantly faster during the erosion at high temperatures, as compared to low ones. The large-scale surface width in this experiment increased, following  $w(t) \simeq t^\beta$ , with the exponent  $\beta \simeq 0.3$  observed over the entire range of measurements at  $T = 725$  K. On the other hand, they found no scaling in the lower temperature regimes, such as  $T = 625$  K. The roughness exponent  $\alpha$  was found to be  $\simeq 0.38 \pm 0.03$ . On the basis of their observations, the authors concluded that, on the large scales, the surfaces become rougher at higher temperatures than at low ones. Similar conclusions

on the temperature dependent character of scaling of the surface width were subsequently drawn in [27]. Moreover, a sharp transition between the scaling regimes in ion-bombardment of Ge(0 0 1) surfaces with 1 keV Xe-ions was observed at  $T_c = 488$  K. The regimes above and below  $T_c$  are characterized by the dynamic scaling exponents  $\beta$  with absolute values  $\simeq 0.4$  and  $\simeq 0.1$ . The roughness evolution of Si(1 1 1) surfaces bombarded by low-energy (500 eV) Ar<sup>+</sup> ions at  $T = 610$  K was studied in [28], using the STM. It was found that the roughness evolution is not described by the diffusion bias-induced roughening and the rough morphology is consistent with early time behavior of the noisy KS equation [34]. Measured roughness exponent was found to be  $\alpha \simeq 0.7$ , and the dynamic exponent  $\beta \simeq 0.25$ , in agreement with numerical simulations of the noisy KS equation [35–37]. It must be noted that the effect of temperature on the evolution of ion-sputtered surfaces is not understood yet and there is no theory which would describe the observed in experiments temperature dependent transitions between different scaling regimes. Additional work on both theory and simulations sides is clearly required to understand the effects of temperature on the irradiated surface evolution.

A number of Monte Carlo simulation studies of the ion-erosion induced surface roughening were recently reported, complementing the available experimental results. Thus, Koponen et al. [45–47] reported on the simulation studies of the roughening of ion-bombarded surfaces. Amorphous carbon surfaces, bombardment by 5-keV Ar-ions, were studied using Monte Carlo simulations in [45,46]. The diffusive relaxation mechanism of the “Wolf-Villain” [42] type was incorporated in the model to study the surface smoothing effects. A wide range of the primary ion incidence angles from 0° to 60° was investigated. It was found that the roughness exponent varies with the angle of incidence, being  $\alpha \simeq 0.37\text{--}0.45$ , for normal incidence, while  $\alpha \sim 0.25$ , for the angle of incidence close to 60°, was observed. In general, the roughness was observed to decrease with the angle of incidence and to be relatively insensitive to the relaxation mechanism employed in the simulations. The growth exponent  $\beta$  was observed to be

nearly independent of the angle of incidence with  $\beta \simeq 0.3$ , over the whole range of the studied angles. On the other hand, it was found to be strongly dependent on the relaxation mechanism and to demonstrate the values  $z \simeq 3.2\text{--}4.0$ , characteristic for the diffusion-controlled processes, in the range of temperatures up to 900 K. In their subsequent studies [47], the roughening of the ion-bombarded carbon surfaces by  $\text{Ar}^+$ - and  $\text{Xe}^+$ -ions were undertaken, for three different incident ion energies of 2, 5 and 10 keV. The study confirmed all the previous findings on the roughness and growth exponent dependence on the angle of incidence and the relaxation mechanism. Additionally, the authors found that the roughness exponent depends strongly on the incident ion penetration depth,  $a$ , with dependence being well approximated by the following linear relation:

$$\alpha = (0.011 \text{ nm}^{-1})a \cos \theta, \quad (6)$$

where  $a$  is the incident ion penetration depth, and  $\theta$  is the angle of incidence.

In summary, experimental studies and computer simulations of the process of ion bombardment have shown that the ion-sputtered surfaces can be well described in terms of the roughness and dynamic exponents, within the framework of the kinetic roughening theory [30]. However, this understanding is a recent development and, in particular, the characterization of surfaces using scaling concepts became standard only in the last few years. Consequently, there was not any attempt taken to study the effect of surface morphology on the sputter yields. We believe that the present work will be of much use to guide such studies.

#### 4. Theory of ion sputtering

Ion bombardment of solids with energetic particles causes the erosion of target material's surfaces. The erosion rate is characterized by the sputtering yield,  $Y$ , defined as the average number of atoms leaving the surface of a solid per incident particle. The theory of ion sputtering, based upon the microscopic considerations of the processes taking place in the bulk of the bombarded mate-

rial, was developed by Sigmund [54,55]. Making use of the hypothesis that the sputtering yield of a polycrystal (amorphous material) can be calculated by assuming random slowing down throughout the cascade, he derived a general expression for the yield as a function of the ion-target and target-target cross-sections as well as atomic binding energies in the bulk of the target material and on the surface. One of the practically important results obtained by Sigmund is the deposited energy distribution function, which was found to have the Gaussian form

$$E(\mathbf{r}_\perp, z) = \frac{\epsilon}{(2\pi)^{3/2} \sigma \mu^2} \exp \left\{ -\frac{z^2}{2\sigma^2} - \frac{x^2 + y^2}{2\mu^2} \right\}. \quad (7)$$

Here,  $\epsilon$  is the kinetic energy of an incident ion,  $\sigma$  and  $\mu$  are the widths of the deposited energy distribution along the  $z$ - (chosen parallel to the incident ion beam direction) and  $x$  ( $y$ )-axis, respectively. The parameters  $\sigma$  and  $\mu$  are material dependent and vary with the physical properties of the target material and the incident ion energy. Deviations of the deposited energy distribution from the Gaussian form (see Eq. (7)) occur mainly when  $M_1 \geq M_2$ , where  $M_1$  is the mass of the projectile and  $M_2$  is the mass of the target material atom. As was shown in the theoretical studies by Sigmund [54,55] and Winterbon [56], the electronic stopping (i.e. the inelastic scattering) does not affect much the shape of deposited energy distribution. Moreover, subsequent Monte Carlo simulations of the sputtering process validated both the deposited energy and the damage distribution forms [1–3]. The comparison of the predictions of the Sigmund's theory of ion sputtering with experimental results have shown that the theory describe well the qualitative behavior of the backsputtering yields and, in many cases, a good quantitative agreement was found. In general, computation of the sputter yield, using Eq. (7) requires a knowledge of the mean path of an incoming ion, traveling inside the bulk of a target material (often referred to as penetration depth). It was shown that the penetration depth can be expressed in terms of the parameters characterizing the target material and the incoming ion energy as follows:

$$a(\epsilon) = \frac{1-m}{2m} \gamma^{m-1} \frac{\epsilon^{2m}}{nC_m}. \quad (8)$$

Here,  $n$  is the target atom density,  $\gamma$  is a constant of the order of unity,  $C_m$  is a constant dependent on the parameters of the interatomic interaction potential [54] and  $m = m(\epsilon)$  is a factor, which varies slowly from  $m = 1$ , at high energies, to  $m = 0$ , at very low energies. It must be emphasized that, in the region of intermediate energies,  $m = 1/2$ , and the penetration depth behavior with the incoming ion energy can be approximated well by the linear dependence,  $a(\epsilon) \sim \epsilon$ . Note that, in general, the deposited energy distribution is defined by the energy deposition depth and not the penetration depth,  $a$ . On the other hand, these quantities are of the same order of magnitude and, therefore, in the following, we assume that the estimates for  $a$  can be used to approximate the energy deposition depth.

In the framework of the Sigmund's theory of ion sputtering, the local yield from a target material surface element  $ds$  can be computed using

$$Y(\mathbf{r})ds = AE(\mathbf{r})ds, \quad (9)$$

where  $Y(\mathbf{r})ds$  is the total number of the target atoms leaving the surface element  $ds$ , located at a distance  $\mathbf{r}$  on the target material's surface from the point of impact of the projectile, and  $E(\mathbf{r})$  the energy deposited by the incoming ions at a point  $\mathbf{r}$ , taken per unit volume. The material constant  $A$  depends on the surface binding energy and the scattering cross-sections [54,55], the exact expression being

$$A = \left\{ \frac{3}{4\pi^2} \right\} \frac{1}{U_o C_o n^2}, \quad (10)$$

where  $U_o$  is the surface binding energy and  $C_o$  is a constant proportional to the square of an effective inter-atomic interaction potential. Thus, the knowledge of the material constants, the penetration depth and the widths of deposited energy distribution allows one to compute the sputter yields for an arbitrary target material. Such calculations, for the flat surfaces, were performed, for instance, in [54] and shown to provide a reasonable description of the sputtering process. It should be noted, however, that, despite the fact that the

Sigmund's theory is known to describe adequately various aspects of the ion sputtering, it also has well known limitations. The most important of such limitations are listed below.

(a) The theory was derived for amorphous materials and may not provide a fully adequate description of the crystalline targets.

(b) The assumption of random slowing down and of an arbitrary collisions works satisfactory only at the intermediate and high energies  $\epsilon \sim 1-100$  keV, while it breaks down at the low energies.

(c) The surface binding energy  $U_o$  brings in a number of uncertainties, which may affect the quantitative results of the theory. Thus, it may undergo significant changes in the process of ion-erosion, caused by the ion-induced amorphization of the near-surface regions of the target material and by the changes in the local surface chemistry in these regions. It should also be emphasized that, in general, the binding energy is local surface curvature dependent. Thus, if the surface profile is not a slowly varying function (as in the case of ripple structures), it may introduce additional uncertainties in the value of binding energy.

## 5. Theoretical approach

### 5.1. General expression for the yield

The physical process taking place during the ion bombardment of solid targets with energetic particles, is illustrated schematically in Fig. 1. An incoming ion strikes the rough target surface at point  $P$ , penetrates the target's interior and stops at a distance  $a$ , at point  $O$ , after all its kinetic energy is dissipated due to the elastic and non-elastic interactions with the atoms of the target material. The energy deposited by an incoming ion is distributed in the interior of the target material and the near-surface region. The transfer of the deposited energy to an arbitrary point  $A$  on the target material surface causes the erosion of the target's surface characterized by the erosion velocity (or the erosion rate),  $v$ . Below, we derive the general expression for the erosion velocity. Let the surface profile be given by  $z = h(x, y)$ . We

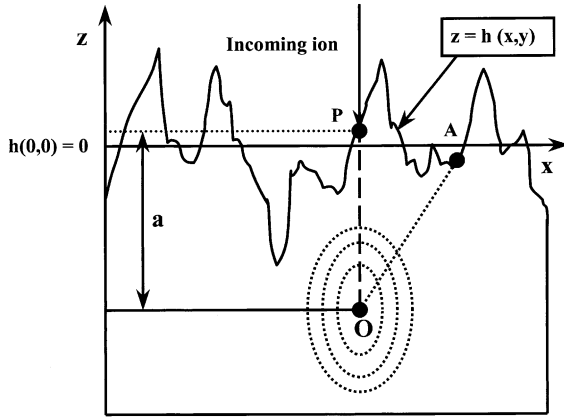


Fig. 1. Schematic illustrating the sputtering process and the geometry of the model system. Following a straight trajectory (solid line in the cartoon), the ion penetrates an average distance  $a$  inside the solid (dotted line), after which it spreads out its kinetic energy. The energy decreases with the distance from the point  $O$ , the dotted curves indicating schematically the equal energy contours. The energy released at point  $O$  contributes to the surface erosion at point  $A$ .

define the reference frame as follows: the  $z$ -axis is chosen to be parallel to the direction of the incident ion beam, while the  $x$ - and  $y$ -axis are located in the plane perpendicular to it, i.e. in the target's surface plane. Note that we consider only the case of normal incidence. The scattering events, caused by an incoming ion, take place in the region of the target material with characteristic length,  $a_e$ , which is the average energy deposition depth (usually, it is of the order of the penetration depth,  $a$ ). Following the Sigmund's theory [54,55], we assume that the energy deposited at an arbitrary point  $A$  on the surface by an incoming ion can be approximated by the Gaussian distribution (see Eq. (7)) and the local erosion rate of the target surface is proportional to the energy deposited at the point  $A$  by *all bombarding ions*. Since there are many incoming ions, reaching the target's surface per unit time (the number of ions per second, per surface area is called fluence and is one of the controlled parameters in the experiments involving the ion bombardment), the erosion rate at the point  $A$  is expressed as

$$v = A \int_{\mathcal{R}} d\mathbf{r}_{\perp} E(\mathbf{r}_{\perp}, h(x, y)) \Phi(\mathbf{r}_{\perp}, h(x, y)). \quad (11)$$

Here, the integration is performed over the region  $R$ , covering all points, at which the deposited energy contributes to the erosion rate at a generic point  $A$  on the surface, and  $\mathbf{r}_{\perp} = (x, y)$ . The function  $\Phi(\mathbf{r}_{\perp}, h(x, y))$  accounts for the corrections to the uniform incident ion flux  $J$ , due to the local surface tilt angle. The most general expression for the local flux for surfaces with non-zero local curvature can be represented by the following form (note that we consider the case of *normal* incidence):

$$\begin{aligned} \Phi(x, y, h(x, y)) \\ = J \cos \left\{ \arctan \left( \sqrt{(\nabla_x h(x, y))^2 + (\nabla_y h(x, y))^2} \right) \right\}. \end{aligned} \quad (12)$$

Now, it is straightforward to obtain the expression for the sputter yield, which can be used to compute the yields from an arbitrary surface with a non-planar geometry given by  $h(x, y)$  in the local coordinate frame. Indeed, in the most general form, the yield is given by

$$Y = \frac{vn}{\langle J \rangle}, \quad (13)$$

where  $n$  is the density of the target atoms and  $\langle J \rangle$  is the average incident ion flux,  $\langle J \rangle = \langle \Phi(x, y, h(x, y)) \rangle$ .

## 5.2. Ion-sputtering of the self-affine surfaces

In general, the set of Eqs. (11)–(13) allows to compute the sputter yield as a function of the parameters characterizing the surface roughness and the incident ion beam, for an arbitrary target material, provided the surface profile can be approximated reasonably well with an analytical function  $z = h(x, y)$ , and this function and the first derivatives of  $h(x, y)$  all exist. It is known, however, that the profiles of random (self-affine) surfaces cannot be expressed in terms of analytical functions and, therefore, such cases have to be treated by other means. In the following, we show how the self-affine surfaces can be described using the basic concepts of modern statistical mechanics. It is well established by now that random interfaces can be characterized well by the height–height correlation

function, that scales with the two-dimensional coordinate vector,  $\mathbf{r}_\perp$ , as  $\langle [h(\mathbf{r}_\perp) - \bar{h}(0)]^2 \rangle \sim (r_\perp)^{2\alpha}$ , where we defined  $r_\perp = |\mathbf{r}_\perp|$ , and by the height probability distribution,  $P(\mathbf{r}_\perp, h)$ . Without loss of generality, in the following, we chose  $h(0, 0) = 0$ . Then, the probability that the surface height at a point  $\mathbf{r}_\perp = (x, y)$  is  $h(x, y)$  is given by the Gaussian distribution of the form [30]

$$P(\mathbf{r}_\perp, h) = \frac{1}{\sqrt{2\pi w^2(r_\perp, \xi)}} \exp \left\{ -\frac{h^2(x, y)}{2w^2(r_\perp, \xi)} \right\}, \quad (14)$$

where  $r_\perp = |\mathbf{r}_\perp|$  and  $w(r_\perp, \xi)$  is the surface width (see Eq. (5), in Section 2). Consequently, instead of performing the integration of Eq. (13) over a well-defined surface topology,  $h(x, y)$ , as implicit in Eq. (11), we take an *average over all the possible surface configurations*, weighting them with probability distribution  $P(\mathbf{r}_\perp, h)$ . It should be noted, that the sputter yields for a flat surface can readily be obtained from Eq. (13), by using  $P(x, y) = \delta(h(x, y) - h_o)$ . Furthermore, the local incident ion flux depends on the gradients of the local surface profile. Consequently, the averages has to be also taken over local surface profile gradients, which we weight with the probability distribution  $P_g(\mathbf{r}_\perp | \nabla_x h(x, y), \nabla_y h(x, y))$ , for the local surface gradients. Taking the corresponding averages, we obtain the following expression for the yield function, which can be used to calculate the total yields from a surface with self-affine morphology:

$$Y = \frac{AnJ}{\langle \Phi(\mathbf{r}_\perp, z) \rangle} \int_{\mathcal{H}} \int_{\mathcal{H}} \int_{-\infty}^{\infty} d\mathbf{r}_\perp dh \mathcal{D}(\nabla_x h) \mathcal{D}(\nabla_y h) \times \cos \left\{ \arctan \left( \sqrt{(\nabla_x h(x, y))^2 + (\nabla_y h(x, y))^2} \right) \right\} \times E(\mathbf{r}_\perp, (h-a)) P(\mathbf{r}_\perp, h) P_g(\mathbf{r}_\perp | \nabla_x h(x, y), \nabla_y h(x, y)) \quad (15)$$

which can be, for further convenience, rewritten as

$$Y = \frac{An}{\langle \Phi(\mathbf{r}_\perp, z) \rangle} \int_{\mathcal{H}} \int_{-\infty}^{\infty} d\mathbf{r}_\perp dh \times E(\mathbf{r}_\perp, (h-a)) \times P(\mathbf{r}_\perp, h) \langle \Phi(\mathbf{r}_\perp, \nabla_x h(x, y), \nabla_y h(x, y)) \rangle. \quad (16)$$

In the process of derivation of Eq. (16), we assumed that the local coordinate dependent surface

height probability distribution,  $P(\mathbf{r}_\perp, h)$ , and the probability distribution for the height gradients (with our choice of the coordinate system  $P_g(\mathbf{r}_\perp | \nabla_x h(x, y), \nabla_y h(x, y))$ ) are not coupled, which is consistent with the self-affine nature of rough surfaces. Moreover, the ion flux depends only on the gradients of the surface profile  $\nabla_x h(x, y)$  and  $\nabla_y h(x, y)$  and not on the height itself. Consequently, the following expression for the local surface gradient corrected flux can readily be obtained:

$$\langle \Phi(\mathbf{r}_\perp, h) \rangle = J \int_{\mathcal{H}} \mathcal{D}(\nabla_x h) \mathcal{D}(\nabla_y h) \times \Phi(\mathbf{r}_\perp, \nabla_x h(x, y), \nabla_y h(x, y)) \times P_g(\mathbf{r}_\perp | \nabla_x h(x, y), \nabla_y h(x, y)). \quad (17)$$

Given the mentioned above decoupling, it is clear that the average flux in the numerator cancels out with the average flux in the denominator of Eq. (16). Combining Eqs. (16) and (17), we obtain the following expression for the sputter yield:

$$Y = An \int_{\mathcal{H}} \int_{-\infty}^{\infty} d\mathbf{r}_\perp dh E(\mathbf{r}_\perp, (h-a)) P(\mathbf{r}_\perp, h). \quad (18)$$

Further, using the expressions for the deposited energy and height probability distributions, and performing the integral over the polar angle, we obtain

$$Y = \frac{An\epsilon}{(2\pi)^{1/2} \sigma \mu^2} \int_0^\infty r dr dh \frac{1}{(2\pi)^{1/2} w(r, \xi)} \times \exp \left\{ -\frac{h^2}{2w(r, \xi)^2} \right\} \exp \left\{ -\frac{(h-a)^2}{2\sigma^2} - \frac{r^2}{2\mu^2} \right\}, \quad (19)$$

where we introduced a new notation:  $r = r_\perp$ .

After performing the integral over  $h$ , the expression for the total yield can be reduced to the following form:

$$Y = \frac{An\epsilon}{(2\pi)^{1/2} \mu^2} \int_0^\infty r dr \frac{1}{\sqrt{(w^2(r, \xi) + \sigma^2)}} \times \exp \left\{ -\frac{r^2}{2\mu^2} \right\} \exp \left\{ -\frac{a^2}{2(w^2(r, \xi) + \sigma^2)} \right\}. \quad (20)$$

To proceed further, we include the functional form of the surface width into Eq. (20). For a kinetically roughened surface, the scaling of the width can be written as

$$\begin{aligned} w^2(r, \xi) &= \langle [h(\mathbf{r}) - \bar{h}(0)]^2 \rangle \\ &= w_{\text{sat}} \left( \frac{r}{\xi} \right)^{2\alpha} f \left( \frac{r}{\xi} \right), \end{aligned} \quad (21)$$

where  $f$  follows  $f(u \rightarrow 0) \sim 1$  and  $f(u \rightarrow \infty) \sim (u)^{2\alpha}$ . As it was discussed in Section 3, the roughness exponent  $\alpha$  varies insignificantly for different materials and incident ions. In our calculations we use  $\alpha = 0.5$ , the value, which is close to the one obtained from the scaling analysis of the KPZ equation [32] and supported by the experimental findings (see Section 3). Using Eq. (21), we finally obtain the yield as a sum of two integrals:

$$Y = \left( \frac{An\epsilon}{(2\pi)^{1/2}\mu^2} \right) (I_1 + I_2), \quad (22)$$

where

$$\begin{aligned} I_1 &= \int_0^\xi r dr \frac{1}{\sqrt{(w_{\text{sat}}^2 (r/\xi)^{2\alpha} + \sigma^2)}} \exp \left\{ -\frac{r^2}{2\mu^2} \right\} \\ &\quad \times \exp \left\{ -\frac{a^2}{2(w_{\text{sat}}^2 (r/\xi)^{2\alpha} + \sigma^2)} \right\}, \end{aligned} \quad (23)$$

$$\begin{aligned} I_2 &= \frac{\mu^2}{\sqrt{(w_{\text{sat}}^2 + \sigma^2)}} \exp \left\{ -\frac{a^2}{2(w_{\text{sat}}^2 + \sigma^2)} \right\} \\ &\quad \times \exp \left\{ -\frac{\xi^2}{2\mu^2} \right\}. \end{aligned} \quad (24)$$

The expression for the sputtering yield from a flat surface can readily be deduced from the above set of equations and is represented by the following analytical form:

$$Y(0) = \left( \frac{An\epsilon}{\sqrt{(2\pi)\sigma}} \right) \exp \left( -\frac{1}{\epsilon_1^2} \right), \quad (25)$$

where we assume that the widths of the deposited energy distribution are linear functions of the penetration depth, i.e.  $\sigma = \epsilon_1 a$  and  $\mu = \epsilon_2 a$ . In the following, we use this quantity to normalize the sputter yield functions to uncover the relative effect of the surface roughness on the yield. Note

that the yield from a flat surface is independent of incident ion energy, for high and intermediate energies, since  $\sigma \sim \epsilon$  in this regime.

In the limit of small values of  $w_{\text{sat}}$ , we can expand Eqs. (22)–(24) in terms of small parameter  $w_{\text{sat}}/a$ , keeping terms up to the second order. We find that, in the initial stages of the roughening process, the yield is a quadratic function of the saturation width,  $w_{\text{sat}}$ , the exact expression being

$$\begin{aligned} Y &= \frac{An\epsilon}{\sqrt{(2\pi)\sigma}} \exp \left\{ -\frac{1}{2\epsilon_1^2} \right\} \\ &\quad \times \left[ 1 + \left( \frac{w_{\text{sat}}}{a} \right)^2 \left( \frac{1}{\epsilon_1^4} - \frac{1}{\epsilon_1^2} \right) \frac{\sqrt{(2\pi\mu^2)}}{2\xi} \right. \\ &\quad \left. \times \left\{ 1 - \sqrt{\frac{2\mu^2}{\pi\xi^2}} \exp \left\{ -\frac{\xi^2}{2\mu^2} \right\} \right\} \right]. \end{aligned} \quad (26)$$

Note that the flat surface result can be recovered from Eq. (26) by taking  $w_{\text{sat}} \rightarrow 0$  and/or  $\xi \rightarrow \infty$  limit.

## 6. Results and discussion

In this section, we present our results on the roughness-induced sputter yield modifications. To study the effect of the surface roughness on the yield, we integrate the set of Eqs. (22)–(24) numerically, obtaining the yield as a function of the surface width,  $w_{\text{sat}}$ , the correlation length,  $\xi$ , and the incident ion penetration depth,  $a$ . To proceed with numerical solution of Eqs. (22)–(24), first the parameters contained in the equations and the ranges of the parameter's variations have to be judiciously chosen. In our model, the parameters, characterizing the surface roughness are selected to match closely the experimental data. On the other hand, the parameters, describing the energy deposited by an incident ion are chosen in a following way. We use the assumption of the linear relation between energy distribution widths  $\sigma$  and  $\mu$  and the incident ion penetration depth,  $a$ , i.e.  $\sigma = \epsilon_1 a$  and  $\mu = \epsilon_2 a$  (see Section 4, for detail discussion). The coefficients  $\epsilon_1 = 1/2$  and  $\epsilon_2 = 1/4$  are selected to obtain an anisotropic energy distribution [1–3]. The ranges of parameter's variations are chosen following the experimental work

by Eklund et al. [20]. In general, the values of the penetration depth, corresponding to the incident ion with energy  $\epsilon$ , is usually obtained using standard Monte Carlo simulations of the high-energy impact processes [57]. In our model calculations the roughness parameters are considered to be independent quantities, with no functional dependence of any form between them assumed. We note that, in general, the roughness parameters span a wide region of values, depending on the particular realization of sputtering conditions, such as the incident ion energy, ion flux and fluence, and the surface temperature. This justifies our choice to employ wide regions of parameter's variations in our model calculations.

In Fig. 2, the behavior of the normalized sputter yield,  $Y(w_{\text{sat}})/Y(0)$ , as a function of the saturation width,  $w_{\text{sat}}$ , is shown for different values of the primary ion penetration depth,  $a$ . The yield is normalized to the flat surface result,  $Y(0)$ . In all studied cases, the correlation length is fixed at  $\xi = 21$  nm. As Fig. 2 demonstrates, the yield

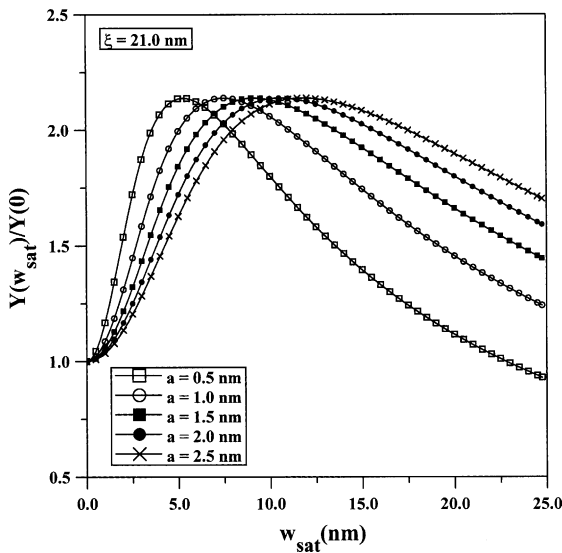


Fig. 2. Normalized yield,  $Y(w_{\text{sat}})/Y(0)$ , is plotted as a function of the saturation width,  $w_{\text{sat}}$ . The value of the correlation length is fixed at  $\xi = 21$  nm. Different curves in the figure correspond to different penetration depths,  $a$ : (1)  $a = 0.5$  nm (open circles), (2)  $a = 1.0$  nm (open squares), (3)  $a = 1.5$  nm (filled circles), (4)  $a = 2.0$  nm (filled squares), (5)  $a = 2.5$  nm (crosses). The lines are shown to guide the eye.

function behavior is qualitatively similar for all considered values of  $a$ . In general, two different regimes in the yield behavior can be discriminated. First such regime is characterized by an enhanced yields, as compared to the flat surface result, which demonstrate an increase with the saturation width. The regime is operative in the region of small values of  $w_{\text{sat}}$ . This behavior of the yield has a simple geometric explanation. Indeed, the behavior of the yield function is largely defined by the surface area regions, which are within the effective cut-off radius of the deposited energy distribution, defined by the magnitude of the penetration depth. The increase in  $w_{\text{sat}}$  leads to the corresponding increase in the effective surface area. If all sputtering conditions are the same, a larger surface area is known to lead to increased yields [55]. Note that qualitatively similar behavior of the yield function is also observed for the rippled surfaces [58], in the regime of small ripple amplitudes. The growth of the yield function with  $w_{\text{sat}}$  continues up to a certain point, which is defined by the magnitudes of both the correlation length and the penetration depth. At the peak points, the deviations of the yields from the flat surface result exceed 200%. The rate of increase of the yield function is strongly dependent on the penetration depth: the rate of growth is stronger for smaller values of  $a$ . Moreover, the positions of the peak of the yield function peak shifts to the region of larger values of  $w_{\text{sat}}$ , as the magnitude of  $a$  increases.

In the initial stages of roughness development, the yield follows a quadratic law as a function of the saturation width (see Eq. (26), in Section 5.2). As we have previously shown in [52], Eq. (26) provides a good approximation for the yield function in this regime. We note that, while the magnitude of the surface width can, in general, be much larger than  $a$ , for many systems the quadratic regime is the most important experimentally. For example, in [20],  $w_{\text{sat}}$  varies from 0 to 10 nm, and  $\xi$  covers the region from 0 to 25 nm. Consequently, the first 25–50% of the experimentally relevant sputtering range is well described by the quadratic law. Furthermore, most of the technologically important sputtering methods require much less erosion. Thus, for these experiments, the entire process will be described by the

quadratic dependence on the surface width. Note that, as follows from Eq. (26), there exist a regime, where the yield function decreases with the saturation width below the flat surface value even in the initial stages of the roughening process. It corresponds to the  $\xi \leq \mu$  limit. We do not study this regime in depth, since such parameter choice falls into contradiction with the available experimental data on surface roughening. It should be emphasized, however, that judicious choice of parameters in the models of surface roughness induced yield modifications is of prime importance for adequate description of the sputtering yields.

The second regime in the yield function behavior, observed in Fig. 2, corresponds to the large values of  $w_{\text{sat}}$ . When  $w_{\text{sat}} \gg a$ , the yield decreases with  $w_{\text{sat}}$ , approximately following  $Y \sim 1/w_{\text{sat}}^2$  dependence. Indeed, as the gradients of the height variations grow (corresponding to a wider height probability distribution), the region  $R$ , which includes all ions contributing to the deposited energy at the point  $A$  on the surface and defined by the effective cut-off in the energy distribution function, cover smaller surface portion, as compared to the region of small values of  $w_{\text{sat}}$ . This leads to decreases in the average erosion rate. It is readily understood that, when  $w_{\text{sat}}$  exceeds the penetration depth, there are parts of the surface that are close to the energy source (the points where the ion was deposited), thus enhancing the yield, while other parts become more distant, effectively suppressing it. The portion of the latter increases with increasing  $w_{\text{sat}}$ . Note that, in the limit of extremely large  $w_{\text{sat}}$  (and for small values of the penetration depth), the yield can be suppressed by the surface roughness below the flat surface value. This behavior is observed in Fig. 2, in the case  $a = 0.5$  nm. The transition between the enhanced and suppressed yields as well as the observed strong dependence on the value of penetration depth can also be explained on the basis of a complex interplay between the yield enhancement by the growing effective surface area and the suppression by the effective cut-off radius.

To further our understanding of the yield behavior with  $w_{\text{sat}}$ , in Fig. 3, we show the normalized yield,  $Y(w_{\text{sat}})/Y(0)$ , dependence on the saturation width, plotted for different values of the

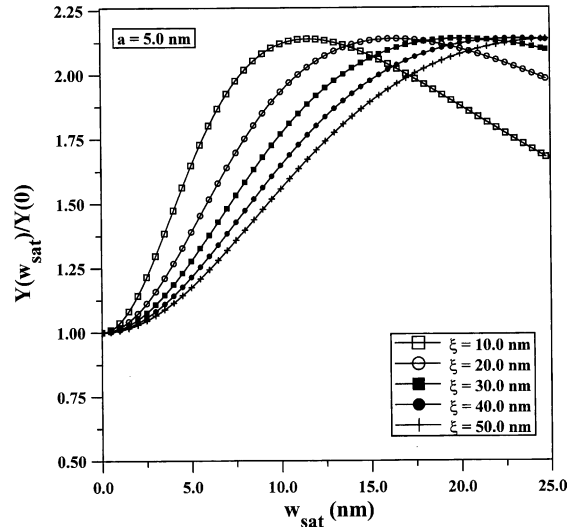


Fig. 3. Normalized yield,  $Y(w_{\text{sat}})/Y(0)$ , is plotted as a function of the saturation width,  $w_{\text{sat}}$ . The value of the penetration depth is fixed at  $a = 5.0$  nm. Different curves in the figure correspond to different values of the correlation length,  $\xi$ : (1)  $\xi = 10$  nm (open squares), (2)  $\xi = 20$  nm (open circles), (3)  $\xi = 30$  nm (filled squares), (4)  $\xi = 40$  nm (filled circles), (5)  $\xi = 50$  nm (crosses). The lines are shown to guide the eye.

correlation length,  $\xi$ . The penetration depth is fixed at  $a = 5.0$  nm. The behavior of the yield function in this case also demonstrates two characteristic regimes. The yield increases with the saturation width, for small values of  $w_{\text{sat}}$ , while it becomes a decreasing function of it, in the limit of large values of the saturation width. The maximum deviations from the flat surface result are approximately the same in all considered cases ( $\approx 200\%$ ). The position of the peak value depends strongly on the surface roughness parameters and the incident ion penetration depth. In the region of small  $w_{\text{sat}}$ , the curves corresponding to the smaller  $\xi$ , demonstrate faster growth and reach their maximums at smaller values of  $w_{\text{sat}}$ . Indeed, the value of  $\xi$  defines how fast the surface profile roughness reaches its saturation value. Consequently, for larger values of  $\xi$ , an effective surface roughness is smaller. Clearly, there exists a value of  $\xi$ , which exceeds the effective cut-off in the deposited energy distribution function. In this case, the effective surface roughness is always smaller than its saturation value. This effect leads

to the observed suppression of the yield (as compared to the peak value) in the limit  $w_{\text{sat}} \ll \xi$ .

In a typical experiment, sputtering starts from a relatively smooth surface of the target material, which is then roughened by the ion bombardment. The interface width is expected to increase with the ion beam fluence,  $\Phi$ , or, alternatively, with the time of exposure to the ion beam,  $t$ , ( $\Phi = Jt$ , where  $J$  is the incident ion flux) as  $w_{\text{sat}} \sim t^\beta$ . As it follows from the foregoing discussion, such an increase in the surface roughness will result in the sputter yield variations. On the other hand, the correlation length also changes with the irradiation time (or fluence). For the self-affine surfaces, the correlation length scales with the time of irradiation following  $\xi \sim t^{1/z}$  relation (see Section 2, for discussion). Consequently, at different stages of the surface roughening process and for different bombarded materials, one would expect to obtain different values of the correlation length at different times of exposure to the ion beam. Note that, this is unlike the ripple wavelength of the periodically modulated surfaces, in which case the ripple wavelength is considered constant for a given realization of the sputtering conditions, up to a certain sputtered depth [16]. Moreover, the constants defining the behavior of the correlation length as a function of the sputtered time are non-universal and depend on nearly every parameter of the system. We can, however, avoid this problem by calculating the yield dependence on the correlation length. Along with the sputter yield dependence on the saturation width, it gives rather complete and experimentally useful information on the yield behavior in the process of surface roughening, where the yield can readily be obtained for any values of the parameters  $w_{\text{sat}}$  and  $\xi$ , if they are monitored in the experiment, and provided that the incident ion penetration depth is known.

In Fig. 4, the normalized sputter yield,  $Y(\xi)/Y(0)$ , dependence on the correlation length is shown for fixed value of the penetration depth,  $a = 5.0$  nm, and different values of the saturation width,  $w_{\text{sat}}$ . As one can see, two types of characteristic behavior are observed, depending on the magnitude of saturation width. For relatively small  $w_{\text{sat}}$ , the yield is a decreasing function of  $\xi$  over the whole region of variations. In this case,

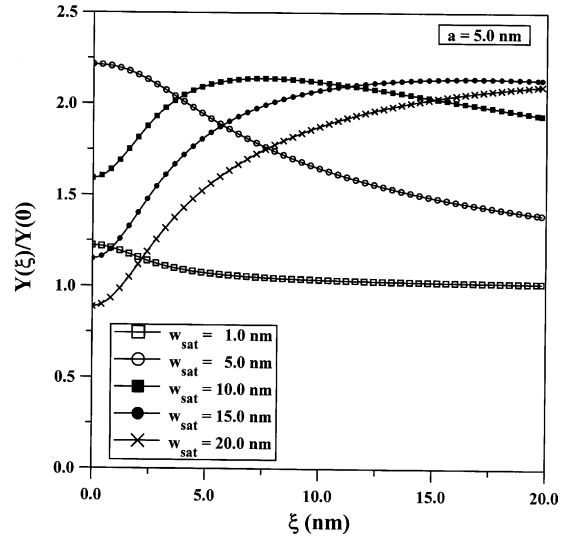


Fig. 4. Normalized yield is plotted as a function of the correlation length,  $\xi$ . The value of  $a$  is fixed at 5.0 nm, and different curves in the figure correspond to different values of  $w_{\text{sat}}$ : (1)  $w_{\text{sat}} = 1.0$  nm (open squares), (2)  $w_{\text{sat}} = 5.0$  nm (open circles), (3)  $w_{\text{sat}} = 10.0$  nm (filled squares), (4)  $w_{\text{sat}} = 15.0$  nm (filled circles), (5)  $w_{\text{sat}} = 20.0$  nm (crosses). The lines are shown to guide the eye.

the dominant effect is the suppression of the effective surface roughness by  $\xi$ . Indeed, as Eq. (21) indicates, when  $\xi$  grows, for fixed  $w_{\text{sat}}$  and  $r$ , the surface width  $w(r, \xi)$  decreases and the scaling function approaches the flat surface limit. Correspondingly, the yield converges to the flat surface result. When the saturation width is large, the behavior of the yield differs from the described above, depending on  $\xi$ . Thus, when  $\xi \leq w_{\text{sat}}$ , the yield increases with  $\xi$ . The rate of increase is approximately the same for all three large (see the curves, corresponding to  $w_{\text{sat}} = 10, 15$  and  $20$  nm) considered values of  $w_{\text{sat}}$ . The yield function reaches the maximum value at  $\xi \simeq w_{\text{sat}}$ . As the correlation length grows further, the yield decreases with  $\xi$ , approaching the flat surface limit from above.

The normalized yield,  $Y(\xi)/Y(0)$ , versus the correlation length, computed for different values of the penetration depth, is shown in Fig. 5. The value of the saturation width is fixed at  $w_{\text{sat}} = 1.0$  nm. In this case, two different types of behavior can be discriminated, depending on  $a$ . In all

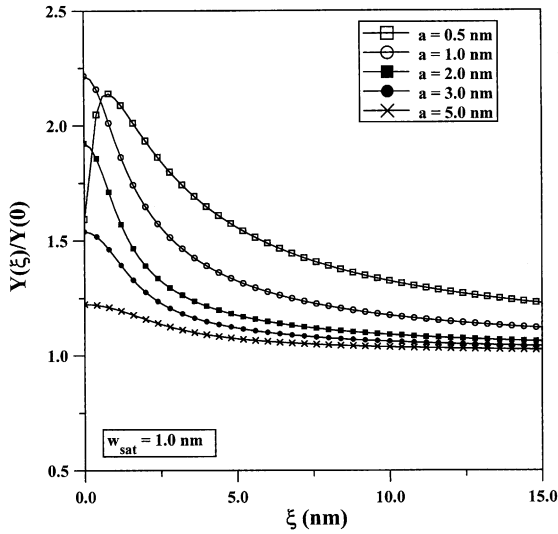


Fig. 5. Normalized yield is plotted as a function of the correlation length,  $\xi$ . The value of  $w_{\text{sat}}$  is fixed at 1.0 nm, and different curves in the figure correspond to different values of the penetration depth,  $a$ : (1)  $a = 0.5$  nm (open squares), (2)  $a = 1.0$  nm (open circles), (3)  $a = 2.0$  nm (filled squares), (4)  $a = 3.0$  nm (filled circles), (5)  $a = 5.0$  nm (crosses). The lines are shown to guide the eye.

considered cases, in the limit of  $\xi \gg w_{\text{sat}}$ , the yield monotonically decreases with the correlation length. Indeed, as follows from Eq. (21), when  $\xi$  grows for fixed  $w_{\text{sat}}$  and  $r$ , the surface width effectively decreases and, therefore, the scaling function approaches the flat surface limit for large values of  $\xi$ . Hence, the yield converges to the flat surface result in this regime. We note that, since for rough surfaces typically  $\xi \gg w_{\text{sat}}$ , we expect that for the experimentally relevant sputtering conditions the yield would decrease with  $\xi$ . On the other hand, the behavior of the yield is penetration depth dependent. While, for large values of  $a$ , the yield monotonically decreases with  $\xi$ , over the whole region of variations, its behavior differs from such for smaller penetration depths (see  $a = 0.5$  nm case). In the latter case, the yield demonstrates growth with the correlation length, in the region of small values of  $\xi$ , reaches a maximum value at a point defined by both  $w_{\text{sat}}$  and the penetration depth, and then monotonically decreases, as  $\xi$  grows further. The effect of the penetration depth on the yield function behavior is discussed below in more details.

To have a complete picture of the effect of surface roughness on the sputter yields, we calculate the yield dependence on the primary ion penetration depth, for different values of the parameters characterizing the surface roughness, i.e.  $w_{\text{sat}}$  and  $\xi$ . According to the Sigmund's theory of sputtering, for intermediate and high energies of the incident ion, the mean ion path in the bulk of sputtered material depends on the incident ion energy as  $a = \epsilon^{2m}$ , where  $m = 1/2$ . Consequently, the yield is independent of the incident ion energy, in this energy regime (see Eq. (26), in Section 5.2). As we show in the foregoing, however, this holds only for the flat surfaces [54,55]. The normalized yield,  $Y(a)/Y(0)$ , dependence on the penetration depth, in the case of self-affine surfaces is shown in Fig. 6. Different curves in the figure correspond to different values of the saturation width,  $w_{\text{sat}}$ , and fixed (at  $\xi = 10.0$  nm) value of the correlation length. The data contained in the region of small  $a$ , however, must be used with a certain caution, since the whole theory works only in the linear

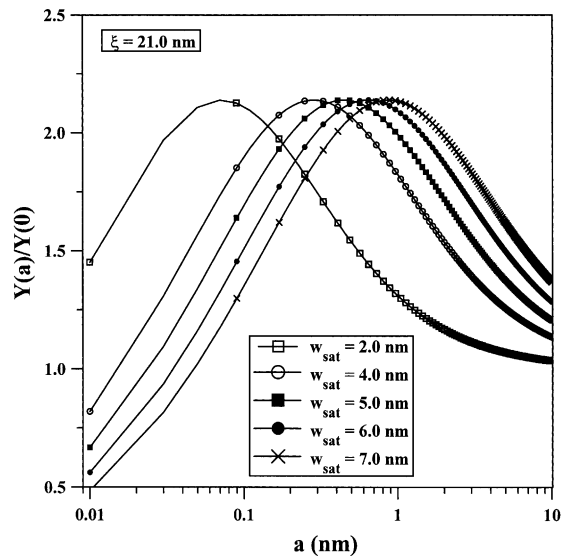


Fig. 6. Normalized yield,  $Y(a)/Y(0)$ , is plotted as a function of the penetration depth,  $a$ . The value of  $\xi$  is fixed at 21 nm. Different curves in the figure correspond to different values of the saturation width,  $w_{\text{sat}}$ : (1)  $w_{\text{sat}} = 2.0$  nm (open squares), (2)  $w_{\text{sat}} = 4.0$  nm (open circles), (3)  $w_{\text{sat}} = 5.0$  nm (filled squares), (4)  $w_{\text{sat}} = 6.0$  nm (filled circles), (5)  $w_{\text{sat}} = 7.0$  nm (crosses). The lines are shown to guide the eye.

cascade regime and, thus, breaks down for the low energies (see Section 4, for detail discussion). On the other hand, different materials have different penetration depths, for a given energy: this follows from the prefactor in the relation between the incident ion energy and the penetration depth. Consequently, the limits of applicability of the model are strongly dependent on particular material properties. Usually these limits as well as the value of penetration depth can be found from Monte Carlo simulations [57]. However, even for realistic ranges of  $a$ , as one can notice, our data shows that there is a transition between different regimes of behavior of the yield function. In the region of small, as compared to  $w_{\text{sat}}$ , values of  $a$ , the yield is an increasing function of  $a$ . The absolute values of the yield in this region are larger for smaller  $w_{\text{sat}}$ , at a given  $a$ . Note that as  $w_{\text{sat}}$  increases, the yield can be suppressed below the flat surface result in the region of small values of  $a$ . This behavior is consistent with our above discussion of the effects of surface roughness on the sputter yields. At a certain value of  $a$ , the yield reaches a maximum value. The position of the peak point shifts towards larger values of  $a$ , as  $w_{\text{sat}}$  increases in magnitude. The flat surface result is recovered in the limit of  $a \gg w_{\text{sat}}$ . In this case, the roughness is nearly absent from the ion's perspective.

In Fig. 7, we show the normalized yield,  $Y(a)/Y(0)$ , as a function of the penetration depth, plotted for fixed value of  $w_{\text{sat}} = 2.0$  nm. Different curves in the figure correspond to different values of the correlation length,  $\xi$ . The behavior of the yield functions, in this case is qualitatively similar to the one observed in Fig. 6. The yield increases in the region of small values of  $a$ , passes through a maximum, and experience a fall-off for large values of  $a$ , approaching the flat surface limit, with  $Y(a)/Y(0) \rightarrow 1$ . The peak value in the yield shifts towards smaller values of  $a$ , as the correlation length increases. The maximum deviations from the flat surface result are approximately the same for all considered values of  $\xi$ . In the region of small  $a$ , the yield is suppressed below the flat surface results. In general, the behavior, observed in Fig. 7, is consistent with the supposition that the yield variations are largely defined by the *effective*

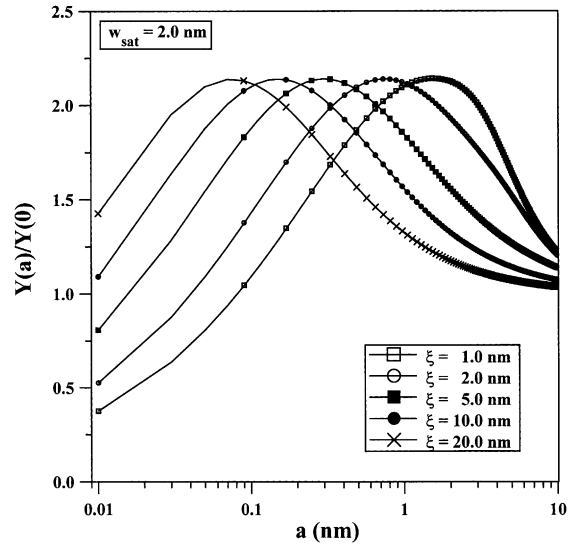


Fig. 7. Normalized yield,  $Y(a)/Y(0)$ , is plotted as a function of the penetration depth,  $a$ . The value of  $w_{\text{sat}}$  is fixed at 2 nm. Different curves in the figure correspond to different values of the correlation length,  $\xi$ : (1)  $\xi = 1.0$  nm (open squares), (2)  $\xi = 2.0$  nm (open circles), (3)  $\xi = 5.0$  nm (filled squares), (4)  $\xi = 10.0$  nm (filled circles), (5)  $\xi = 20.0$  nm (crosses). The lines are shown to guide the eye.

roughness, which is controlled by the correlation length (see Eq. (21)) and the effective cut-off radius.

## 7. Summary and conclusions

In conclusion, we have developed a theoretical model describing the sputtering yield behavior in the case of the self-affine surfaces bombarded with energetic ions. Within the framework of this model, the sputter yields have been computed as a function of the parameters characterizing the roughness of self-affine surfaces (such as the surface width and the correlation length) and the primary ion (penetration depth). We found that the surface roughness development can induce substantial variations in the sputter yields, with magnitude of the effect being dependent on a complex interplay between the parameters characterizing the incident ion beam and the surface roughness. We found that, for small values of the saturation width, the sputter yields increase,

following approximately a quadratic law  $Y \sim w_{\text{sat}}^2$ . This is similar to the case of ripple morphology, where the yield was found to be a quadratic function of the ripple amplitude. As the surface width increases further, the yield reaches a maximum value and then experiences a fall-off. The maximum enhancement in the yield can be as large as  $\approx 200\%$ . In general, the effect of the yield changes by the surface roughness is shown to be strongly dependent on the specifics of the surface roughness and the primary ion beam characteristics. We have found, that *in the experimentally relevant* region of incident ion energies the major effect of the roughness is the enhancement of sputter yields. On the other hand, we have investigated wide ranges of the roughness parameters variations, without specific connections to available at the time experimental data. In a certain range of parameters variations, the yield was found to decrease below the flat surface results. In general, the yield was shown to demonstrate a substantial variation with the correlation length and the penetration depth, where also different regimes in the yield behavior were uncovered. This emphasizes the crucial role, which finest details of the surface morphology play in defining the sputter yields from rough surfaces.

While our model was developed for the single-component systems, the multi-component targets can, in principle, be described within the framework of this approach, if it is modified accordingly [59,60]. Indeed, according to [59], for a binary alloy  $AB$  the yields of the constituents ( $A$  and  $B$ ) can be related through:  $Y_A/Y_B \sim \left(\frac{M_B}{M_A}\right)^{2m} \left(\frac{U_B}{U_A}\right)^{1-2m}$ , where  $Y_{A,B}$  are the sputtering yields for the two species,  $U_{A,B}$  are the binding energies of the species at the target's surface and  $M_{A,B}$  are the masses of the target constituents. Although it is impossible to directly compare the prediction of this model with experimental results, the crude estimates show that this approach can account for the matrix elements of binary alloy reasonably well [59,60]. It should be noted that the model is not capable to describe the erosion of dopants. (To our knowledge, no reasonable approach exist, which adequately describes the sputter yield behavior

for target dopants.) This represents one of the major future challenges to the theory.

Although no direct experimental data exist on the sputter yield dependence on the surface saturation width (or the correlation length), which can be compared with our results in the whole range of roughness parameter variations (such as in [16]), the yield modifications by surface roughness can be considered a confirmed experimental fact. On the other hand, additional experimental work is clearly needed to investigate all the aspects of the problem. Such study would require an investigation of the sputter yields, accompanied by the simultaneous study of the surface morphology, for instance, using the STM. Due to the high interest in surface roughening during MBE growth, a number of experimental techniques have been developed that allow quite precise in situ measurement of the surface width, while experimental techniques providing the yield measurements were in the place for a long time [1–3]. Consequently, it is possible to verify experimentally the width dependence of the yield. Moreover, the main effect lies in the energy and roughness regimes that are relevant under normal experimental conditions. As previous studies have demonstrated [20–23], bombarding a flat surface with ions at low enough temperatures (when the surface diffusion is negligible, and thus the ripple formation can be avoided) roughens the surface, the roughness varying between 0.5 and 100 nm with the increasing fluence. Our study indicate that the peak in the yield (where the roughness generated yield enhancement is the largest, and is easiest to detect) appears for penetration depths between 0 and 60 nm, both within the experimentally reachable ranges. Thus, it is possible to investigate in details the yield behavior near its predicted peak using the existing experimental techniques.

One of the major motivations for investigating the surface roughening effects was the belief that by investigating the major forces acting during roughening can help as either avoid roughness or understand its impact on various technologically important processes. Our study represents a major step in this direction: making use of the fundamental discoveries made in the last decade, it provides rather specific view on the influence of the

roughness on the easily measurable parameter (sputtering yield), and thus contributing to the better understanding of ion beam sputtering, a tool extremely important for both scientific research and technology.

## References

- [1] P.D. Townsend, J.C. Kelly, N.E.W. Hartley, *Ion Implantation, Sputtering and their Applications*, Academic Press, London, 1976.
- [2] R. Behrish (Ed.), *Sputtering by Particle Bombardment*, Vols. I and II, Springer, Heidelberg, Germany, 1981, 1983.
- [3] W. Eckstein, *Computer Simulation of Ion–Solid Interactions* Springer Series in Materials Science, Vol. 10, Springer, Berlin, 1991.
- [4] A. Zalar, *Thin Solid Films* 124 (1985) 223.
- [5] A. Zalar, *J. Vac. Sci. Technol. A* 5 (1987) 2979.
- [6] F.A. Stevie, P.M. Kahora, D.S. Simons, P. Chi, *J. Vac. Sci. Technol. A* 6 (1988) 76.
- [7] K. Wittmaack, *J. Vac. Sci. Technol. A* 8 (1990) 2246.
- [8] S.P. Smith, in: A. Benninghoven, C.A. Evans, K.D. McKeegan, H.A. Storms, H.W. Werner (Eds.), *Secondary Ion Mass Spectroscopy*, Vol. VII, Wiley, New York, 1990.
- [9] E.-H. Cirlin, J.J. Vajo, T.C. Hasenberg, R.J. Hauenstein, *J. Vac. Sci. Technol. A* 8 (1990) 4101.
- [10] E.-H. Cirlin, J.J. Vajo, R.E. Doty, T.C. Hasenberg, *J. Vac. Sci. Technol. A* 9 (1991) 1395.
- [11] A. Karen, K. Okuno, F. Soeda, A. Ishitani, *J. Vac. Sci. Technol. A* 9 (1991) 2247.
- [12] A. Karen, K. Okuno, F. Soeda, A. Ishitani, in: A. Benninghoven, C.A. Evans, K.D. McKeegan, H.A. Storms, H.W. Werner (Eds.), *Secondary Ion Mass Spectroscopy*, Vol. VIII, Wiley, New York, 1990.
- [13] K. Wittmaack, in: D. Briggs, M.P. Seah (Eds.), *Practical Surface Analysis, Ion and Neutral Spectroscopy*, Vol. 2, Wiley, Chichester, 1992.
- [14] E.-H. Cirlin, *Thin Solid Films* 220 (1992) 197.
- [15] A. Karen, Y. Nakagawa, M. Hatada, K. Okuno, F. Soeda, A. Ishitani, *Surf. Interface Anal.* 23 (1995) 506.
- [16] J.J. Vajo, R.E. Doty, E.-H. Cirlin, *J. Vac. Sci. Technol. A* 14 (1996) 2709.
- [17] R.M. Bradley, J.M.E. Harper, *J. Vac. Sci. Technol. A* 6 (1988) 2390.
- [18] R.M. Bradley, E.-H. Cirlin, *Appl. Phys. Lett.* 68 (1996) 3722;  
R.M. Bradley, *Phys. Rev. E* 54 (1996) 6149.
- [19] G. Carter, *Appl. Phys. Lett.* 71 (1997) 3067.
- [20] E.A. Eklund, R. Bruinsma, J. Rudnick, R.S. Williams, *Phys. Rev. Lett.* 67 (1991) 1759.
- [21] E.A. Eklund, E.J. Snyder, R.S. Williams, *Surf. Sci.* 285 (1993) 157.
- [22] J. Krim, I. Heyvaert, C. Van Haesendonck, Y. Bruynseraede, *Phys. Rev. Lett.* 70 (1993) 57.
- [23] H.-N. Yang, G.-C. Wang, T.-M. Lu, *Phys. Rev. B* 50 (1994) 7635.
- [24] X.-S. Wang, R.J. Pechman, J.H. Weaver, *Surf. Sci.* 364 (1996) L511.
- [25] P. Konarski, M. Hautala, *Vacuum* 47 (1996) 1111.
- [26] Z. Csahok, Z. Farkas, M. Menyhard, G. Gergely, C.S. Daroczi, *Surf. Sci.* 364 (1996) L600.
- [27] D.-M. Smilgies, P.J. Eng, E. Landemark, M. Nielsen, *Surf. Sci.* 377 (1997) 1038.
- [28] A.C.-T. Chan, G.-C. Wang, *Surf. Sci.* 414 (1998) 17.
- [29] F. Family, T. Vicsek (Eds.), *Dynamics of Fractal Surfaces*, World Scientific, Singapore, 1991;  
P. Meakin, *Phys. Rep.* 235 (1993) 189;  
T. Halpin-Healy, Y.-C. Zhang, *Phys. Rep.* 254 (1995) 215.
- [30] A.-L. Barabási, H.E. Stanley, *Fractal Concepts in Surface Growth*, Cambridge University Press, Cambridge, 1995.
- [31] L.M. Sander, in: C. Godreche (Ed.), *Solids Far from Equilibrium*, Cambridge University Press, 1990.
- [32] M. Kardar, G. Parisi, Y.-C. Zhang, *Phys. Rev. Lett.* 56 (1986) 889.
- [33] J.M. Kim, J.M. Kosterlitz, *Phys. Rev. Lett.* 62 (1989) 2289;  
B.M. Forrest, L.H. Tang, *J. Stat. Phys.* 60 (1990) 181;  
K. Moser, J. Kertész, D.E. Wolf, *Physica A* 178 (1991) 215;  
T. Ala-Nissila, T. Hjelt, J.M. Kosterlitz, O. Venalainen, *J. Stat. Phys.* 72 (1993) 207.
- [34] Y. Kuramoto, T. Tsuzuki, *Prog. Theor. Phys.* 55 (1977) 356;  
G.I. Sivashinsky, *Acta Astronaut.* 6 (1979) 569.
- [35] S. Zaleski, *Physica D* 34 (1989) 427;  
K. Sneppen et al., *Phys. Rev. A* 46 (1992) 7352;  
F. Hayot, C. Jayaprakash, Ch. Jossierand, *Phys. Rev. E* 47 (1993) 911;  
V.S. L'vov et al., *Nonlinearity* 6 (1993) 25.
- [36] I. Procaccia, M.H. Jensen, V.S. L'vov, K. Sneppen, R. Zeitak, *Phys. Rev. A* 46 (1992) 3220;  
V.S. L'vov, I. Procaccia, *Phys. Rev. Lett.* 69 (1992) 3543;  
V.S. L'vov, I. Procaccia, *Phys. Rev. Lett.* 72 (1994) 307;  
C. Jayaprakash, F. Hayot, R. Pandit, *Phys. Rev. Lett.* 71 (1993) 12;  
C. Jayaprakash, F. Hayot, R. Pandit, *Phys. Rev. Lett.* 72 (1994) 308.
- [37] L. Golubović, R. Bruinsma, *Phys. Rev. Lett.* 66 (1991) 321;  
L. Golubović, R. Bruinsma, *Phys. Rev. Lett.* 67 (1991) 2747 (E);  
R. Cuerno, K.B. Lauritsen, *Phys. Rev. E* 52 (1995) 4853.
- [38] J.G. Amar, F. Family, *Phys. Rev. A* 41 (1990) 3399.
- [39] S.F. Edwards, D.R. Wilkinson, *Proc. R. Soc. London A* 381 (1982) 17.
- [40] J. Villain, *J. Phys. I (France)* 1 (1991) 19.
- [41] D.E. Wolf, *Phys. Rev. Lett.* 67 (1991) 1783.
- [42] D.E. Wolf, J. Villain, *Europhys. Lett.* 13 (1990) 389.
- [43] S. Das Sarma, P.I. Tamborenea, *Phys. Rev. Lett.* 66 (1991) 325.
- [44] R. Bruinsma, in: R. Jullien et al. (Eds.), *Surface Disorder: Growth Roughening and Phase Transitions*, Nova Science, New York, 1992.

- [45] I. Koponen, M. Hautala, O.-P. Sievänen, *Phys. Rev. B* 54 (1996) 13502.
- [46] I. Koponen, M. Hautala, O.-P. Sievänen, *Phys. Rev. Lett.* 78 (1997) 2612.
- [47] I. Koponen, M. Hautala, O.-P. Sievänen, *Nucl. Instr. and Meth. B* 127 (1997) 230.
- [48] I. Koponen, M. Hautala, O.-P. Sievänen, *Nucl. Instr. and Meth. B* 129 (1997) 349.
- [49] Y. Yamamura, C. Mossner, H. Oechsner, *Radiat. Eff.* 103 (1987) 25.
- [50] M.A. Shaheen, D.N. Ruzic, *J. Vac. Sci. Technol.* 11 (1993) 3085.
- [51] M. Kustner, W. Eckstein, V.D.J. Rose, *Nucl. Instr. and Meth. B* 145 (1998) 320.
- [52] M.A. Makeev, A.-L. Barabasi, *Appl. Phys. Lett.* 73 (1998) 1445.
- [53] M.A. Makeev, A.-L. Barabasi, Companion paper.
- [54] P. Sigmund, *Phys. Rev.* 184 (1969) 383.
- [55] P. Sigmund, *J. Mater. Sci.* 8 (1973) 1545.
- [56] K.B. Winterbon, *Radiat. Eff.* 13 (1972) 215.
- [57] J.F. Zeigler, J.P. Biersack, U. Littmark, *The Stopping and Ranges of Ions in Solids, Vol. I*, Pergamon, New York, USA, 1986.
- [58] M.A. Makeev, A.-L. Barabasi, *Appl. Phys. Lett.* 72 (1998) 906.
- [59] R. Kelly, *Surf. Sci.* 100 (1980) 85.
- [60] I.L. Singer, J.S. Murday, J. Comas, *J. Vac. Sci. Technol. A* 18 (1981) 161.